INVITED PAPER *Special Section on Recent Progress in Superconducting Analog Devices and Their Applications*

New Approach of Laser-SQUID Microscopy to LSI Failure Analysis

Kiyoshi NIKAWA[†a)], **Shouji INOUE**[††], ***Nonmembers***, **Tatsuoki NAGAISHI**[†††], ***Member***,
Toru MATSUMOTO[††††], ***Nonmember***, **Katsuyoshi MIURA**[†††††], ***and*** **Koji NAKAMAE**[†††††], ***Members***

SUMMARY We have proposed and successfully demonstrated a two step method for localizing defects on an LSI chip. The first step is the same as a conventional laser-SQUID (L-SQUID) imaging where a SQUID and a laser beam are fixed during LSI chip scanning. The second step is a new L-SQUID imaging where a laser beam is stayed at the point, located in the first step results, during SQUID scanning. In the second step, a SQUID size (A_{eff}) and the distance between the SQUID and the LSI chip (ΔZ) are key factors limiting spatial resolution. In order to improve the spatial resolution, we have developed a micro-SQUID and the vacuum chamber housing both the micro-SQUID and the LSI chip. The A_{eff} of the micro-SQUID is a thousand of that of a conventional SQUID. The minimum value of ΔZ was successfully reduced to 25 μm by setting both the micro-SQUID and an LSI chip in the same vacuum chamber. The spatial resolution in the second step was shown to be 53 μm. Demonstration of actual complicated defects localization was succeeded, and this result suggests that the two step localization method is useful for LSI failure analysis.

key words: *SQUID, laser, LSI chip, failure analysis, defect localization*

1. Introduction

The concept of a scanning laser-SQUID microscope (L-SQUID) which uses the combination of laser beam and SQUID (superconducting quantum interference device) magnetometer was proposed first by Beyer et al. [1]. They applied the L-SQUID to inspect uniformity of impurity in Si wafers. We have proposed to apply the L-SQUID for inspection, monitoring and failure analysis of LSI-chip-defects, and demonstrated inspection and failure analysis of actual LSI chips [2]–[5]. In demonstration of failure analysis, we found that we can localize a single site open defect using L-SQUID without any help of other tools such as CAD-navigation [4], [5]. Other defects, however, such as short defects, multiple site open defects or more complicated defects, could not be localized using L-SQUID.

In this paper, we propose and demonstrate a new approach where we can localize not only open defects but also short defects or more complicated defects.

Manuscript received July 1, 2008.
Manuscript revised September 19, 2008.

[†]The author is with Test and Analysis Engineering Division, NEC Electronics Corporation, Kawasaki-shi, 211-8668 Japan.
[††]The author is with Semiconductor Division, TDI Co Ltd., Yokohama-shi, 222-0033 Japan.
[†††]The author is with Equipment Development Division, Sumitomo Electric System Solutions, Itami-shi, 664-0016 Japan.
[††††]The author is with Systems Division, Hamamatsu Photonics K.K., Hamamatsu-shi, 431-3196 Japan.
[†††††]The authors are with the Department of Information Systems Engineering, Graduate School of Information Science and Technology, Osaka University, Suita-shi, 565-0871 Japan.
a) E-mail: k.nikawa@necel.com
DOI: 10.1587/transele.E92.C.327

2. Laser-SQUID Microscope with SQUID-Scanning Capability

L-SQUID described in [4] and [5] has not SQUID scanning capability. We have added a SQUID scanning capability to our L-SQUID system this time. The effective area (A_{eff}) of the micro-SQUID for scanning which we have developed this time is a thousandth of a conventional SQUID (cf. Appendix A).

2.1 Basic Concept of Conventional L-SQUID and New L-SQUID

Figure 1 shows basic concept of a conventional L-SQUID (a) and a new L-SQUID (b). In the scheme of the conventional L-SQUID, a SQUID magnetometer and a laser beam are fixed during sample scanning. As a consequence, the laser beam scans on the sample. In the scheme of the new L-SQUID, on the other hand, the laser beam stays at a certain point on a sample during SQUID scanning.

The spatial resolution in the conventional L-SQUID scheme is limited by the laser beam diameter. The spatial resolution in the new L-SQUID scheme, on the other hand, is limited by the SQUID size (A_{eff}) and the distance between the SQUID and a sample (ΔZ). The SQUID size and the ΔZ are therefore important factors in the new L-SQUID scheme. In order to achieve high spatial resolution, we have developed a micro-SQUID and a vacuum chamber housing both the micro-SQUID and an LSI chip.

2.2 System Setup

The essence of our L-SQUID system is shown in Fig. 2.

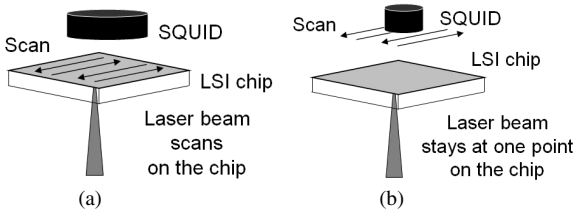

Fig. 1 Conventional L-SQUID and new L-SQUID (a) Conventional L-SQUID: sample scanning, (b) New L-SQUID: SQUID scanning.

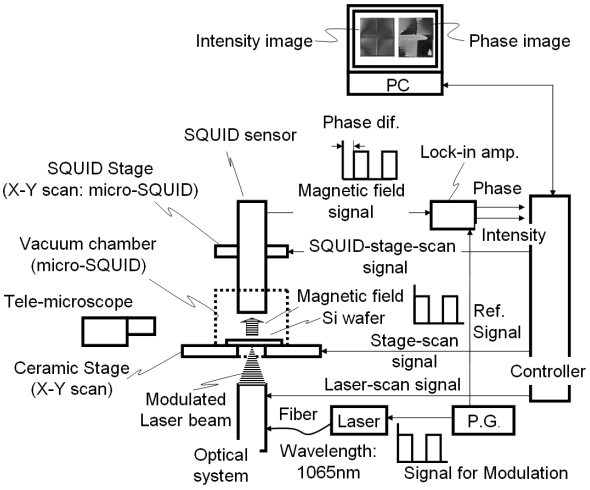

Fig. 2 System setup.

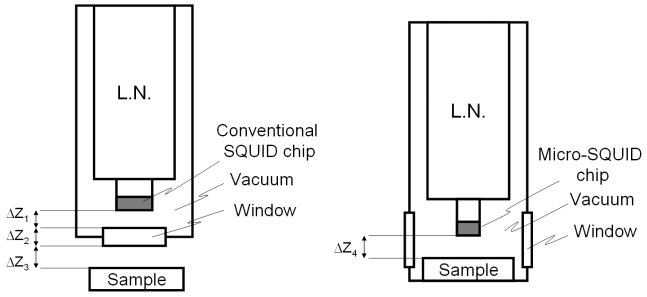

(a) Conventional L-SQUID (b) New L-SQUID

Fig. 3 Configurations of SQUID chips and samples in the conventional L-SQUID scheme and in the new L-SQUID scheme.

When a laser beam is focused at a p-n junction on an LSI chip, a photocurrent is induced and the photocurrent induces very weak magnetic field. The magnetic field is detectable by a DC-SQUID magnetic sensor. The whole system is magnetically and electromagnetically shielded (the shield room is not shown in Fig. 2). In the conventional L-SQUID scheme, a ceramic stage scans when a wide area is scanned, and a laser beam scans when a narrow area is scanned. The SQUID chip in the SQUID sensor module is cooled down to about 77 K using a liquid nitrogen (L.N.) cryostat. The ΔZ ($\Delta Z_1 + \Delta Z_2 + \Delta Z_3$ in Fig. 3(a)) is usually set to about 0.4 mm in the conventional L-SQUID scheme. The ΔZ in the new L-SQUID scheme (ΔZ_4 in Fig. 3(b)), on the other hand, can be set down to 25 μm because a sample is set in vacuum as shown in Fig. 3(b). Figure 4 shows the side view of the SQUID chip and an LSI chip when the ΔZ is 50 μm. The side view can be imaged by tele-microscopes set at two perpendicular positions each other (only one is shown in Fig. 2). The effective area (A_{eff}) of the conventional SQUID chip used in the conventional L-SQUID scheme is 0.2 mm^2. That of the micro-SQUID chip used in the new L-SQUID scheme, on the other hand, is 0.0002 mm^2. The detail of the two types of SQUID chips is described in Appendix A.

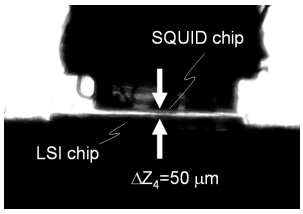

Fig. 4 Side view of the SQUID chip and an LSI chip imaged by the tele-microscope.

As shown in Fig. 2, the laser beam is introduced from the bottom side. We use a 1065 nm wavelength fiber laser which can penetrate a Si substrate and generate photocurrents at p-n junctions near the surface of the Si substrate. The intensity of the laser beam is modulated with an acousto-optic modulator and the resulting modulated SQUID output signal is introduced into a lock-in amplifier. The output signal of the lock-in amplifier is used for imaging intensity and phase. The combination of magnetic shielding and "laser modulation/lock-in" approach makes pico-Tesla-order magnetic signals detectable in micro-Tesla-order magnetic noises in our laboratory.

3. Application to LSI Failure Analysis

3.1 Defective Part Localization by Sample-Scanning (Conventional Approach)

Figure 5 shows a result of a conventional approach where Vdd-open-site is localized by the conventional L-SQUID scheme. The maximum magnetic field (the brightest point) in the intensity images is about 3×10^{-10} T. The sample is designed (layout design) and manufactured using the system of VDEC (VLSI Design & Education Center, the University of Tokyo) based on C7552 circuit of ISCAS'85 benchmark circuits [6]. In Fig. 5, you can see a layout, an optical image, and L-SQUID images. The field of view (FOV) of each image is 1 mm $\times$ 1 mm. In the optical image, the Vdd-open site, which is designed in a no good chip, is shown. By comparing L-SQUID images of good and no good chips, you can clearly find out the differences in both intensity images and phase images. In the intensity image of a no good chip, open site is localized as a dark part between two bright parts. In the phase image of a no good chip, open site is localized as the interface of inverted phases.

We have localized many single-site-open defects using the conventional L-SQUID scheme as shown in Fig. 5 and in [4] and [5]. Other defects such as short or more complicated defects, however, have not been localized by the conventional L-SQUID scheme. In the next section, we would like to propose and demonstrate the new idea of two step localization in order to localize not only open defects but also short defects or more complicated defects.

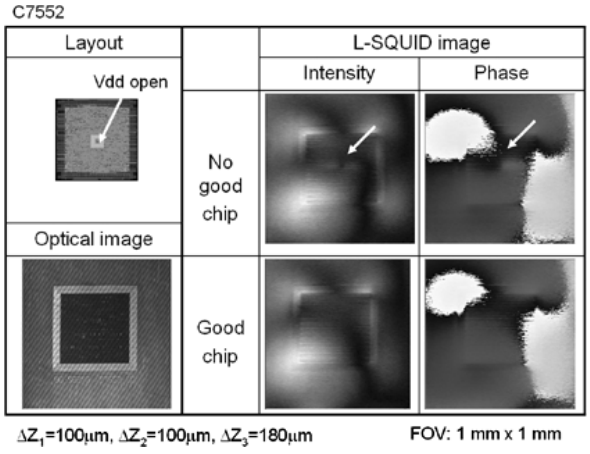

Fig. 5 Vdd-open-site localization by the conventional L-SQUID scheme: The maximum magnetic field (the brightest point) in the intensity images is about 3×10^{-10} T.

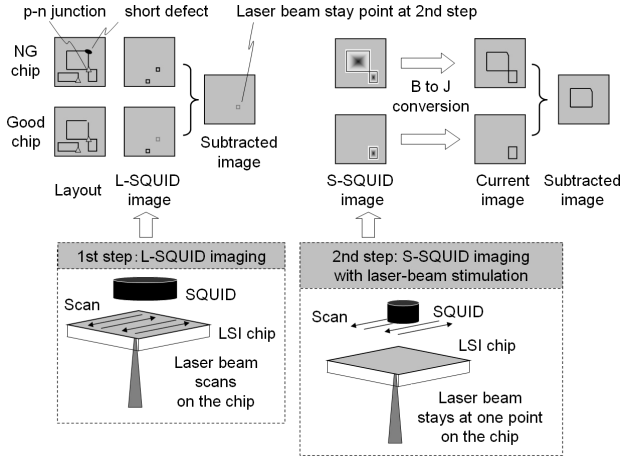

Fig. 6 Main concept of two step localization.

3.2 Defective Part Localization by Sample-Scanning Followed by SQUID-Scanning (New Approach: Two Step Localization)

Figure 6 shows a main concept of two step localization. In the first step, L-SQUID images of both good and no good chips are taken in the conventional L-SQUID scheme. Then a contrast-different part between good and no good chip images is selected as the laser-beam stay point in the second step. In the second step, the laser beam is stayed at the point, determined in the first step, during SQUID scanning. The scanning SQUID images of both good and no good chips are converted into current images using Fourier Transform (see Appendix B). If there are any different parts between two current images, at least two cases are possible. In one case, a short defect must exist at the image different part. In another case, an open defect must exist at the image different part. In the former case, a part of current paths appears in a no good chip image (Fig. 6). In the later case, on the other hand, a part of current paths disappears in a no good chip image: this case is not shown in Fig. 6.

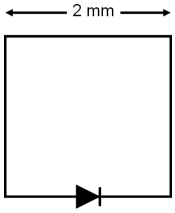

Fig. 7 Test structure used to measure the spatial resolution.

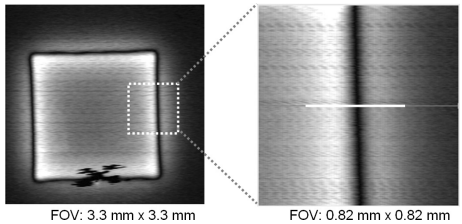

(a) Scanning SQUID intensity images: the maximum magnetic field (the brightest point) in the intensity images is about 5×10^{-8} T.

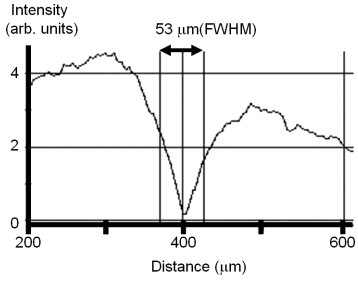

(b) Line profile of the magnetic field intensity along a line shown in the image of (a).

Fig. 8 Scanning-SQUID images and a line profile.

The key factors of the spatial resolution in the second step are ΔZ and A_{eff} as described above. In order to confirm the spatial resolution in the second step, we used a test structure shown in Fig. 7. The test structure made on a Si substrate consists of a p-n junction and a rectangular metal loop. The linewidth of the loop is $2\,\mu$m. A scanning SQUID image when a laser beam is stayed at the p-n junction is shown in Fig. 8(a). The maximum magnetic field (the brightest point) in the intensity images is about 5×10^{-8} T. The line profile of the magnetic field intensity along a line shown in the right image of (a) is shown in (b). In this scanning, we used the micro-SQUID (A_{eff} =0.0002 mm^2) described in Appendix A and set ΔZ to $25\,\mu$m. Figure 8(b) shows that the spatial resolution is $53\,\mu$m (FWHM, full width at half maximum).

In order to demonstrate the two step localization method, we selected the 256MDRAM chip which had been tested electrically by conventional probing and had found out to be stand-by-current failure. Figure 9 shows conventional L-SQUID images of good and no good chips. The maximum magnetic field (the brightest point) in the intensity images is about 1×10^{-9} T. You can clearly see the contrast differences between good and no good chip images. We selected two points indicated by arrows as "1" and "2" in

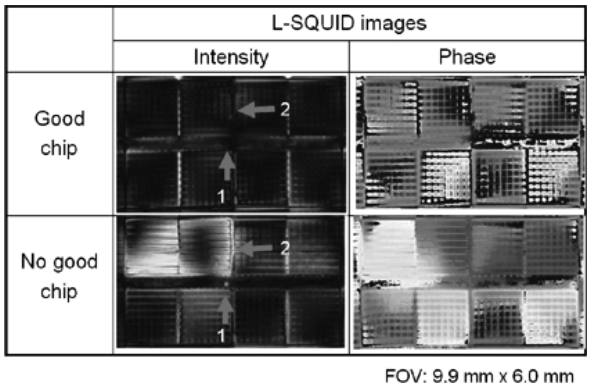

Fig. 9 Conventional L-SQUID images of 256MDRAMs in the first step: The maximum value of the magnetic field (the brightest point) in the intensity images is about 1×10^{-9} T.

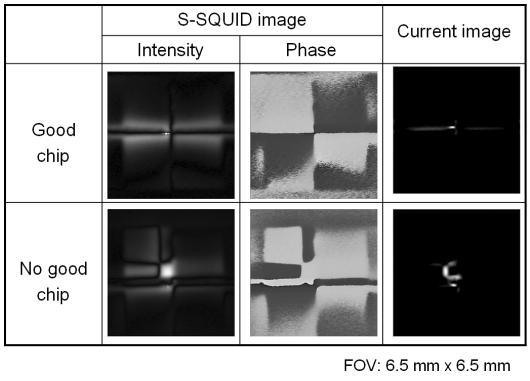

Fig. 10 Scanning SQUID images and converted current image in the second step when a laser beam was stayed at the point "1": The maximum value (the brightest point) in the intensity images is about 7×10^{-8} T, and that in the current images is about 2×10^{-5} A.

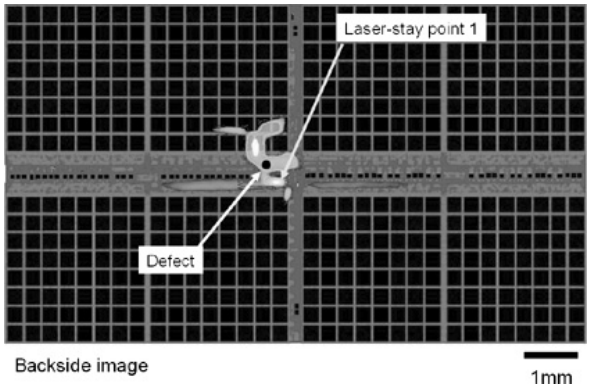

Fig. 11 Overlay of a layout and two current images when a laser beam was stayed at the point "1."

Fig. 9 as the laser-beam stay points in the second step. The point "1" was selected because an especially bright spot was seen only in no good chip image. The point "2," on the other hand, was randomly selected from bright areas in a no good chip. Figure 10 shows the scanning SQUID images and converted current images when laser beams were stayed at the point "1." The maximum value (the brightest point) in the

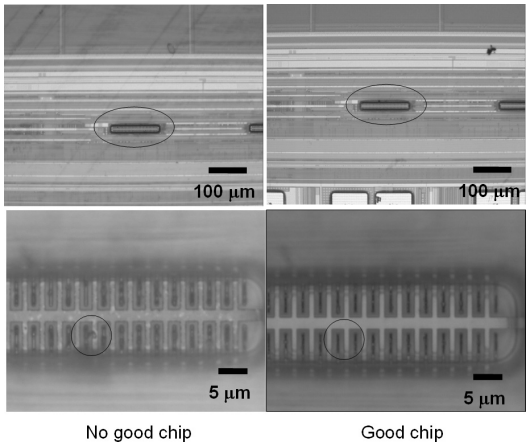

Fig. 12 Optical microscope images of a defective area localized when a laser beam was stayed at the point "1."

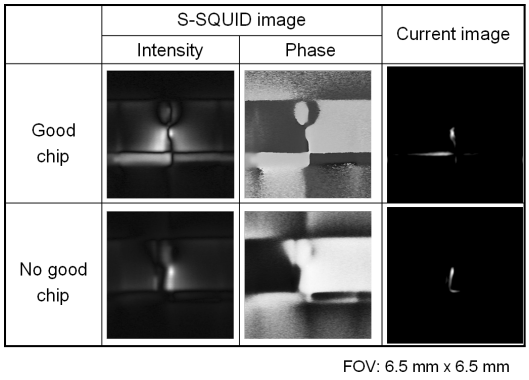

Fig. 13 Scanning SQUID images and converted current images in the second step when a laser beam was stayed at the point "2": The maximum value (the brightest point) in the intensity images is about 1×10^{-7} T, and that in the current images is about 4×10^{-5} A.

intensity images is about 7×10^{-8} T, and that in the current images is about 2×10^{-5} A. Figure 11 shows the overlaid images of two current images (good and no good chips) and a layout of a chip. As shown in Fig. 11, we have successfully localized a defect on the no good chip current path and not on the good chip current path. Optical microscope images showing localized defective area are shown in Fig. 12. You can see a few-μm size defect in the high magnification no good chip image.

Concerning the stay point "2," we have also succeeded to localize a defect. Scanning-SQUID images with converted current images, overlay of current images and a layout, and optical images are shown in Figs. 13, 14, and 15 respectively. The maximum magnetic field (the brightest point) in the intensity images in Fig. 13 is about 1×10^{-7} T, and that in the current images is about 4×10^{-5} A. In Fig. 15, you can see a few-tens-μm size defect in no good chip images.

These results suggest that the two step localization method is useful for localization of complicated defective sites on an LSI chip.

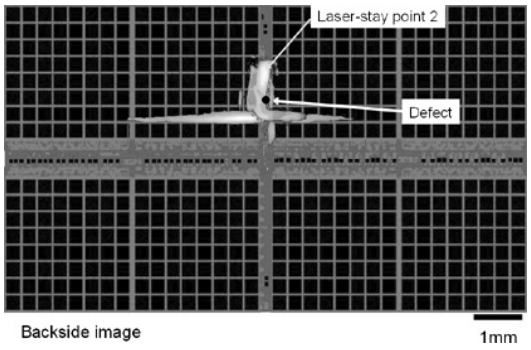

Fig. 14 Overlay of a layout and two current images when a laser beam was stayed at the point "2."

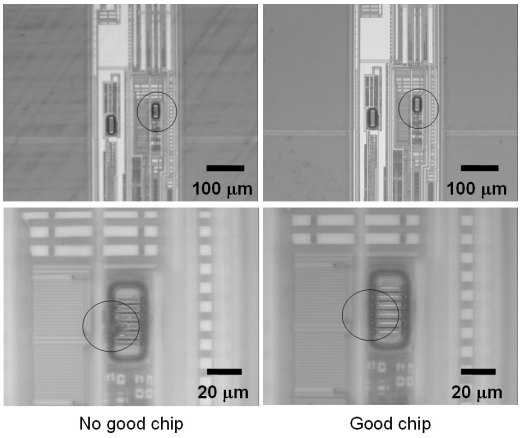

Fig. 15 Optical microscope images of a defective area localized when a laser beam was stayed at the point "2."

4. Summary and Conclusion

We have proposed and successfully demonstrated the two step localization method. In order to improve the spatial resolution in the second step, we have developed the micro-SQUID and the vacuum chamber housing both the micro-SQUID and an LSI chip. The spatial resolution was shown to be about 50 μm. A few-μm size and a few-tens-μm size defects have been localized on a 256MDRAM chip by applying the proposed method.

These results suggest that the two step localization method proposed in this paper is useful for localization of complicated defective sites on an LSI chip.

Acknowledgments

A part of this research and development was supported by JST (Japanese Science and Technology Agency). A part of the VLSI chips in this study has been fabricated in the chip fabrication program of VLSI Design and Education Center (VDEC), the University of Tokyo.

References

[1] J. Beyer, H. Matz, D. Drung, and T. Schurig, "Magnetic detection of photogenerated currents in semiconductor wafers using superconducting quantum interference devices," Appl. Phys. Lett., vol.74, pp.2863–2865, 1999.
[2] K. Nikawa, "Laser-SQUID microscopy as a novel tool for inspection, monitoring and analysis of LSI-chip-defects," IEICE Trans. Electron., vol.E85-C, no.3, pp.746–751, March 2002.
[3] K. Nikawa, "6 Laser-SQUID microscope for LSI chip defect analysis," in Applications of HTCS SQUIDs, in Voltex Electronics and SQUIDs, ed. T. Kobayashi, H. Hayakawa, and M. Tonouchi, pp.224–233, Springer, 2004.
[4] K. Nikawa, "3.2 scanning laser-SQUID for IC testing," in M. Tonouchi, A. Fujimaki, K. Tanabe, K. Enpuku, K. Nikawa, and T. Kobayshi, "Recent topics in high-Tc Superconductive Electronics," Jpn. J. Appl. Phys., vol.44, no.11, pp.7740–7742, 2005.
[5] K. Nikawa and S. Sakai, "Newly-developed scanning laser-SQUID microscope," Proc. 31 Int'l Sympo. Testing and Failure Analysis, pp.14–20, USA, Nov. 2005.
[6] F. Brglez and H Fujiwara, "A neutral netlist of 10 combinational benchmark circuits and a target simulator in FORTRAN," Proc. Int'l Sympo. Circuits and Systems (ISCAS), pp.695–698, Japan, May 1985, http://www.cbl.ncsu.edu/benchmarks/
[7] R.C. Black, A. Mathai, F.C. Wellstood, E. Dantsker, A.H. Miklich, D.T. Nemeth, J.J. Kingston, and J. Clarke, "Magnetic microscopy using a liquid nitrogen cooled $YBa_2Cu_3O_7$ superconducting quantum interference device," Appl. Phys. Lett., vol.62, no.17, pp.2128–2130, 1993.
[8] T.S. Lee, E. Dantsker, and J. Clarke, "High-transition temperature superconducting quantum interference device microscope," Rev. Sci. Instrum., vol.67, no.12, pp.4208–4215, 1996.
[9] B.J. Roth, N.G. Sepulveda, and J.J.P. Wikswo, "Using a magnetometer to image a two-dimensional current distribution," J. Appl. Phys., vol.65, no.1, pp.361–372, 1989.
[10] S. Chatraphorn, E. Fleet, F. Wellstood, and L. Knauss, "Noise and spatial resolution in SQUID microscopy," IEEE Trans. Appl. Supercond., vol.11, no.1, pp.234–237, March 2001.

Appendix A: Two Types of SQUID Chips: Conventional SQUID and Micro-SQUID

Two types of SQUID chips shown in Fig. A· 1 are used in this study. Both are the square washer type with different sizes and shapes. The conventional type SQUID has millimeter order washer size. The other is the small SQUID with 20 μm square washer size: a micro-SQUID [7], [8].

The details of the SQUID designs are shown in Fig. A· 2. The main portion of the conventional type SQUID is given in Fig. A· 2(a). It has 4 μm wide and 250 μm length slit which focuses the magnetic fluxes. The other slits to make junctions with 2 μm wide are elongated to one side of the washer. Full picture of the micro-SQUID is given in Fig. A· 2(b). The micro-SQUID has 10 μm by 10 μm hole with 20 μm by 20 μm washer and the slits located opposed position to make 2 μm wide junctions. Superconducting thin films are $HoBa_2Cu_3O_{7-x}$ on $SrTiO_3$ substrates and the junctions are the step-edge type. The differences of the parameters and the characteristics are given in Table A· 1.

Appendix B: Conversion of Magnetic Field to Electric Current

In this appendix, we show a method to calculate the electric

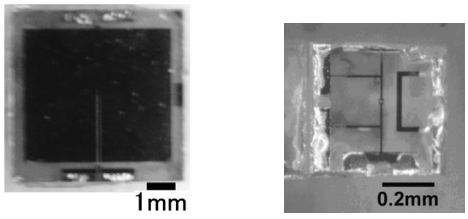

(a) (b)

Fig. A· 1 Optical micrographs of SQUIDs (a) Conventional type SQUID, (b) Micro-SQUID. In (a), no feed back line is on the chip and the junctions which are hardly recognized are located closed to the center of the chip. In (b), square shape part closed to the center of the chip is the SQUID and the feed back line is located on the right side of the SQUID.

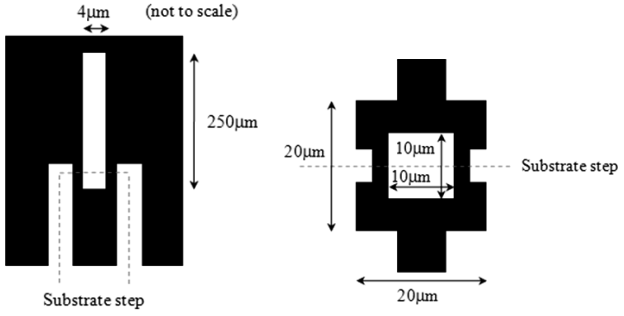

(a) (b)

Fig. A· 2 Schematic diagrams of SQUIDs (a) Conventional type SQUID, (b) Micro-SQUID. The main portion of the conventional type is given in (a) and the full picture of the micro-SQUID is given in (b).

Table A· 1 Differences of the SQUID parameters and the characteristics of the SQUIDs.

	Conventional SQUID	Micro-SQUID
Outer size	5mm X 4.5mm	20μm X 20μm
Substrate size	6mm X 6mm	500μm X 500μm
Inductance (estimated)	50pH	32pH
Effective area (estimated)	0.2mm^2	0.0002mm^2
Modulation voltage	∼10 μV	∼20 μV
Flux noise (@10Hz)	20μΦ_0/Hz$^{1/2}$	30μΦ_0/Hz$^{1/2}$

current density vector from the measured magnetic field. It is based on the method proposed in [9], [10] and sensitivity distribution of a SQUID is introduced in it.

When it is assumed that the current is flowing only in a very thin sheet of thickness d that exists in the x-y plane, two-dimensional (2D) Fourier transformation of current density $j_x(k_x, k_y)$ and $j_y(k_x, k_y)$ can be calculated by the following equations [8], [9]:

$$j_x(k_x, k_y) = -\frac{i2}{\mu_0 d} e^{kz} \frac{k_y}{k} b_z(k_x, k_y, z) \cdot f(k), \quad (\text{A}\cdot 1)$$

$$j_y(k_x, k_y) = +\frac{i2}{\mu_0 d} e^{kz} \frac{k_x}{k} b_z(k_x, k_y, z) \cdot f(k). \quad (\text{A}\cdot 2)$$

where k_x and k_y are the x and y components of the spatial angular frequency, $k = \sqrt{k_x^2 + k_y^2}$, i is the imaginary unit ($i = \sqrt{-1}$), μ_0 is the magnetic permeability of free space, z is a distance from the sheet to the SQUID, $b_z(k_x, k_y, z)$ is 2D Fourier transformation of the measured magnetic field, and $f(k)$ is a low-pass filter function to suppress high-frequency noise. Therefore, the current density vector $\boldsymbol{J}(x, y)$ can be obtained by applying inverse 2D Fourier transformation to Eqs. (A· 1) and (A· 2).

As the low-pass filter $f(k)$, the Hamming window function expressed by the following equation is used in this study:

$$f(k) = \begin{cases} 0.54 - 0.46 \cos\left(\dfrac{2\pi k}{K}\right) & (0 \le k < K) \\ 0 & (K < k) \end{cases}, \quad (\text{A}\cdot 3)$$

where K is a cut-off frequency. When K is small, the special resolution of the obtained current density distribution becomes coarse. Contrary, when K is large, serious artifacts appear in the current density distribution while the special resolution becomes fine. The optimal value of K is determined depending on the amount of noise in $b_z(k_x, k_y, z)$.

In the method described above, the size of a SQUID is assumed to be very small and negligible. However, as is described in the Appendix A, the size of a SQUID is in a range from a few tens of micrometers to millimeters. It can not be always ignored. We introduced a sensitivity distribution function $S(x, y)$ of a SQUID to the conversion method. The measured value $\widehat{B}_z(x, y, z)$ of the z component of magnetic field $B_z(x, y, z)$ is convolution of $S(x, y)$ and $B_z(x, y, z)$. From the convolution theory, 2D Fourier transformation of $\widehat{B}_z(x, y, z)$ is expressed as

$$\widehat{b}_z(k_x, k_y, z) = s(k_x, k_y) \cdot b_z(k_x, k_y, z) \quad (\text{A}\cdot 4)$$

where $s(k_x, k_y)$ is 2D Fourier transformation of $S(x, y)$. From Eqs. (A· 1), (A· 2), and (A· 4), the following equations can be obtained:

$$j_x(k_x, k_y) = -\frac{i2}{\mu_0 d} e^{kz} \frac{k_y}{k} \widehat{b}_z(k_x, k_y, z) \cdot \frac{f(k)}{s(k_x, k_y)}, \quad (\text{A}\cdot 5)$$

$$j_y(k_x, k_y) = +\frac{i2}{\mu_0 d} e^{kz} \frac{k_x}{k} \widehat{b}_z(k_x, k_y, z) \cdot \frac{f(k)}{s(k_x, k_y)}. \quad (\text{A}\cdot 6)$$

As the sensitivity distribution function, the Gaussian distribution is assumed in this study:

$$S(x, y) = \frac{1}{\sqrt{2\pi}\sigma} \exp\left(-\frac{x^2 + y^2}{2\sigma^2}\right), \quad (\text{A}\cdot 7)$$

and the standard deviation σ is optimized by comparing the measured magnetic field of a simple-structured specimen with calculated one.

Kiyoshi Nikawa received the B.S. and M.S. degrees in material science, and Ph.D. degree from Osaka University, Osaka, Japan. He has been with the NEC group, Japan, where he has been working on reliability engineering for Si integrated circuits, especially, on bipolar devices, electromigration, failure analysis using a focused ion beam, a electron beam, and a laser beam. He is an author or a co-author of more than 200 technical papers and more than twenty books. He was a vice-president of Reliability Engineering Association of Japan (REAJ), and is a council of the REAJ, a committee of the institute of LSI Testing, a member of the Japan Society of Applied Physics (JSAP), IEEE, and Electron Device Failure Analysis Society (EDFAS).

Shouji Inoue received the B.S. degree in telecommunication engineering from Tokai University, Kanagawa, Japan in 1978. In 1979, he joined TDI Co. Ltd. where he worked on the development of the space equipment. Since 1985, he has been working on reliability engineering, especially failure analysis of LSIs.

Tatsuoki Nagaishi received his B.S. degree in Physics from Osaka University in 1985, M.S. degree in Materials Science and Engineering from Stanford University in 1989, and Ph.D. degree from Osaka University in 2005. He joined Sumitomo Electric Industries, Ltd. in 1985. Since1989, he was engaged in the R&D of high temperature superconducting materials. He developed high quality and large area high Tc thin films using excimer laser deposition. Along with the thin film development, he started the development of high Tc SQUID and commercialized the high Tc SQUID systems in the fields of education, non-destructive evaluation, geophysical exploration and others.

Toru Matsumoto received the B.E. degree in image science from Chiba University, Chiba, Japan in 1988. He joined Hamamatsu Photonics K.K. in 1988 and worked on the development of the inspection system using image sensor. In 2002, he developed the scanning laser SQUID microscope with Dr. Kiyoshi Nikawa. Since 2004, he has been working on the development of the failure analysis system for LSIs using image sensor, SQUID and other sensor.

Katsuyoshi Miura is a associate professor in the Department of Information Systems Engineering, Graduate School of Information Science and Technology, Osaka University, Osaka, Japan. He received the B.E. and M.E. degrees in electronic engineering, and Ph.D. degree in information systems engineering from Osaka University. His research interests include methods and systems of VLSI testing, fault diagnosis and failure analysis.

Koji Nakamae is a professor in the Department of Information Systems Engineering, Osaka University, Osaka, Japan. His current interests lie in LSI fault diagnosis, signal and image processing, and the analysis of the economics of VLSI manufacturing, including test costs. Nakamae received the B.E., M.E., and Ph.D. degrees in electronic engineering from Osaka University.